Seabed Instability due to Flow Liquefaction in the Fraser River Delta

by

AnnajiRao V. Chillarige[1]

N.R. Morgenstern[2]

P.K. Robertson[2]

H.A. Christian[3]

[1] Geotech Consultants International, Inc.
2265 Lee Road, Suite 221-A
Winter Park, Florida 32789
USA

[2] University of Alberta
Department of Civil Engineering
Edmonton, Alberta, Canada
T6G 2G7

[3] Geological Survey of Canada (Atlantic), P.O. Box 1006
Dartmouth, Nova Scotia, Canada
B2Y 4A2

Submitted to

Canadian Geotechnical Journal

January 1997

Abstract

Seabed Instability due to Flow Liquefaction in the Fraser River Delta

AnnajiRao V. Chillarige, N.R. Morgenstern, P.K. Robertson, H.A. Christian

Liquefaction failures of loose sand deposits can be a major concern for the stability of coastal structures. An investigation to evaluate the possible contributions of different triggering mechanisms in a major liquefaction failure that occurred in 1985 at the mouth of the Main Channel of the Fraser River has been carried out using steady state concepts.

Potential triggering mechanisms for initiating the 1985 liquefaction flow slide, such as sedimentation, surface waves and low tides are evaluated. The analysis shows that rapid sedimentation generates shear stresses on the slope but may not initiate flow liquefaction failures. The evaluation of the effect of surface waves in causing deep seated liquefaction flow slides indicates that no significant porewater pressures accumulate due to the surface waves in the region. Low tides cannot initiate failure in submerged, fully saturated sands. However, gas induces desaturation of the sediment which can induce residual pore pressures in the sediments during low tides. It is postulated that the combination of loose sediments, small amounts of gas and low tides contribute to the triggering of flow liquefaction failures in the delta. These failures lead to retrogressive flow slides.

Key words: Liquefaction, steady state, rapid sedimentation, surface waves, low tides, gaseous sediments.

Introduction

Liquefaction flow slides are recurrent phenomena in active river deltas. These flow slides can be triggered by dynamic effects, such as earthquakes, surface waves, blasting and vibrations due to pile driving operations and by static effects such as tidal changes, and sedimentation. The occurrence of flow slides due to static effects has usually been unexpected. Terzaghi (1956) referred to the phenomenon of sudden or static liquefaction of loose sands by minor triggering mechanisms as spontaneous liquefaction. Several cases of reported flow slides in coastal marine deposits have been presented in a companion paper by Chillarige et al. (1997). The spontaneous liquefaction flow slides in coastal sediments generally occurred in fine silty sands during low tide conditions. While explaining the causes of coastal flow slides in the Netherlands that occurred regularly over many years, Terzaghi (1956) suggested that the collapse of the metastable structure of the fine silty sands was caused by the seepage pressure of the ground water which returned to the ocean during the receding tide. However, an explanation for static liquefaction flow slides in coastal zones is not altogether accepted and additional trigger actions have been suggested. Different environmental processes such as rapid sedimentation, low tides, surface waves, gas in the sediments, currents, dredging operations and loading from ship's propellers may trigger or contribute to the initiation of liquefaction flow slides in river deltas. Researchers studying the causes of triggering of flow slides in river deltas have not quantified the contributions of the triggering mechanisms.

Five known liquefaction flow slides occurred near Sand Heads in the Fraser River Delta (FRD) on the west coast of Canada between 1970-1985 (McKenna et al., 1992). The mechanisms that are mentioned above are believed to contribute to the triggering of these failures. An investigation has been carried out using steady state concepts to quantify the

contributions of the triggering mechanisms for a liquefaction flow slide that occurred in 1985 in the FRD.

This paper presents a review of steady state concepts in explaining the liquefaction phenomenon. It also evaluates the contributions of different environmental processes in triggering the flow slide and provides a rational and quantitative explanation for the 1985 liquefaction flow slide in the FRD. Companion papers (Christian et al., 1997; Chillarige et al., 1997) describe the field investigation and subsequent characterization of the loose sandy sediments at the mouth of the Main Channel of the Fraser River.

Background for Liquefaction Phenomenon

An approach developed by Castro (1969) improves our understanding of the phenomenon of liquefaction. He defined liquefaction as the strain softening and collapse in undrained shear of a loose sand to an ultimate state, called steady state. While differentiating different mechanisms of liquefaction, Robertson (1994) referred to this aspect of liquefaction as flow liquefaction. If the gravitational shear stresses of a soil deposit are larger than the steady state resistance of the deposit, liquefaction leading to flow deformations can occur. When the flow deformation occurs on a slope, a flow slide can develop. In level ground conditions, the soil can lose its bearing capacity.

At the steady state of deformation, a mass of soil deforms at constant volume, constant shear stress, and constant velocity (Poulos, 1981). The void ratio at steady state is the critical void ratio as defined by Casagrande (1936) and Koppejan et al. (1948). Liquefaction can take place in loose saturated or near saturated sands with the void ratio higher than the critical void ratio.

The steady state of any sand can be represented by a curve in the void ratio - effective confining stress - deviatoric stress space (e -p' -q space) where:

$p' = \frac{1}{3}(\sigma_1' + \sigma_2' + \sigma_3')$ and $q = (\sigma_1' - \sigma_3')$.

The in-situ state of a soil deposit can be described in the e-p'-q space, and the response of the soil deposit can be obtained by following the appropriate stress path in that space. In normal practice, a steady state line (SSL) is represented by the projections of the curve on to the e -p' plane and the p'-q plane (Figure 1). The projection of the SSL in the e-p' plane can be approximated as a straight line on a logarithmic abscissa. The SSL in the p'-q plane is also a straight line passing through the zero coordinate. The SSL in the e-p' plane separates the in-situ state of sand into regions which are loose and contractant at large strains from those which are dense and dilatant at large strains. Ishihara (1993) presented results of undrained tests on very loose Toyoura sand samples, exhibiting essentially zero residual undrained shear strength (steady state strength). The void ratio corresponding to the zero residual strength is called the " Threshold Void Ratio". This void ratio marks essentially the beginning of the steady state line. The in-situ void ratio at very shallow depths of a very loose sand deposit may correspond to this threshold void ratio. During undrained shear loading, this soil can have zero steady state strength.

The shear behavior of the soil is very much influenced by the effective confining pressure. A soil of low relative density can behave in a contractant manner at higher confining pressures or in a dilatant manner at low confining pressures (Kramer and Seed, 1988). Castro and Poulos (1977) state that the position of the steady state line is a fundamental soil property. Been et al. (1991) also state that the steady state line for a given sand is independent of stress path, sample preparation and initial density, implying that the steady state is unique for a void ratio regardless of whether it is reached by drained or undrained loading.

Morgenstern (1967) indicated that the initiation of flow liquefaction failures was consistent with the mobilization of the undrained shear strength of the loose soils. For a contractant sand at large strains whose in-situ driving shear stresses are higher than the available undrained shear strength, there exists a potential for flow liquefaction of the sand which may lead to a catastrophic failure. However, for a dilatant sand where the undrained shear strength is greater than the driving shear stress, flow liquefaction may not be a concern.

As mentioned previously, flow liquefaction is due to the collapse and strain softening in undrained shear of the metastable soil structure resulting in the generation of large pore pressures. During the collapse of the contractant material, the permeability of the material must be sufficiently low to impede the drainage of the excess pore pressures for flow liquefaction to occur. Hence, coarse grained gravelly deposits may not be subjected to flow liquefaction. However, some percentage of fine material in the gravel deposits may impede drainage during collapse. Lade (1993) indicated that no statically triggered liquefaction flow slides are observed in saturated cohesionless soils with permeabilities greater than 10^{-4} m/sec. Dawson et al. (1992) observed that liquefaction flow slides occurred in mine waste dumps with permeabilities of about 10^{-4} m/sec.

Collapse Surface Concept

From the results of laboratory tests on different sands, Sladen et al. (1985a) introduced the concept of a collapse surface to serve as a triggering criterion for flow liquefaction. They state that the necessary condition to trigger flow liquefaction is that the soil state must reach the collapse surface. The undrained effective stress paths of contractant (loose) sand samples which are consolidated to the same void ratio, but sheared at different initial confining pressures converge to the same ultimate steady state at large

strains. The peak deviatoric stress of all the stress paths fall on an approximate straight line that passes through the steady state strength of the samples. Sladen et al. (1985a) referred to this line as the collapse line (see Figure 2). Different undrained stress paths of the same material tested at different initial void ratios yield collapse lines of approximately the same slope, but terminate at different ultimate states on the steady state line. All these collapse lines in the e-p'-q space generate a collapse surface at which the collapse of a loose saturated material is initiated by undrained loading. The collapse surface constitutes a trigger criterion regardless of whether it is approached by monotonic or cyclic loading. There is a potential risk for a soil to liquefy when its in-situ state is close to the collapse surface. Any small disturbance could lead to flow liquefaction, if the soil is sufficiently loose, its in-situ state is close to collapse and the in-situ shear stresses are larger than the ultimate undrained shear strength.

Contractant State Boundary (CSB)

Later studies on sands have revealed a state boundary surface which controls the behavior of purely contractant sands at large strains (Alarcon-Guzman et al., 1988; Ishihara et al., 1991). The state boundary surface is the surface enveloping all the undrained effective stress paths of the contractant soil, irrespective of their consolidation stresses and void ratios. A sandy soil cannot exist above the state boundary. Sasitharan (1994) indicated that for triaxial compression the surface can be approximated by parallel straight lines in the p'-q plane for different void ratios and observed that soils are less brittle at higher stress states as the state boundary appears to flatten at higher stresses. Since the state boundary controls the behavior of contractant soils, it can be identified as a Contractant State Boundary (CSB

Sasitharan et al. (1993) presented results from q - constant tests in which the stress path of a loose saturated sand remained in a constant shear stress plane in e-p'-q space and the specimen was brought to failure under fully drained conditions (Figure 3). During the test, the drained stress path attempted to cross the CSB resulting in collapse of the soil structure and the rapid generation of pore pressures. The shear resistance fell along the CSB to the steady state, that is, flow liquefaction. This stress path simulates a rise of the water table in loose sands. During the rise, changes in the stress state of the soil can be induced under drained conditions. However, the deformations associated with the soil collapse increase pore pressures, the soil response becomes undrained and the soil liquefies. This phenomenon has been observed in laboratory modeled flow slides in coal stock piles by Eckersley (1990). The q-constant test path also explains the failures that have occurred in coal mine waste dumps (Dawson et al., 1992). These results demonstrate that undrained loading is not a pre-requisite for flow liquefaction to occur.

Sasitharan (1994) demonstrated in another laboratory test the existence of the CSB. A p' - constant stress path (constant effective mean normal stress path) test was conducted on a loose saturated sand sample with its stress state on the post peak portion of the undrained effective stress path, that is, the sample is on its CSB. The stress path tried to cross the CSB vertically in the p'-q plane (Figure 3), but the stress path stayed on the CSBdue to a decrease in void ratio (e) and reached its steady state at a different void ratio.

The existence of the CSB is also evident from tests on dry sand samples in a constant shear stress plane (Skopek et al., 1993). The stress path is similar to that described by Sasitharan et al. (1993). During the test the shear stress was unchanged (q-constant test) while p' was reducing. The stress path was forced to deflect to remain on the CSB (Figure 3) to accommodate the structural changes (decrease in void ratio) due to the loading and the sample experienced rapid structural collapse on the CSB. The contractant

behavior of the dry sand is consistent with the behavior of loose saturated sand. A saturated sample collapses on the CSB along the q-constant test path, resulting in vigorous generation of pore pressures and flow liquefaction. If the pore pressures are released during the collapse, the stress path re-positions to a more stable stress state either on the state boundary or away from the boundary. An instability exists on the CSB whenever a soil attempts to cross it. All the above tests illustrate that a loose sand cannot exist beyond the contractant state boundary surface.

Application of CSB Concept

Sladen et al. (1985b) explained the flow liquefaction failures of the Nerlerk berms in the Beaufort Sea using the collapse surface concept. The construction of the berm by hydraulic filling brought the in-situ state of the soil to the collapse surface. Additional dumping of the fill resulted in undrained flow slides. Similar observations were made by Lade (1993) for the berm failures. Lade proposed an instability line in the p'-q plane passing through the peaks of undrained stress paths of samples at the same void ratio and through the origin. He concluded that the state of soil in the berms was in the region of instability and undrained failures were initiated due to dumping of berm material. The two arguments by Sladen et al., (1985b) and Lade (1993) agree with the conclusion that the state of the soil in the berms was on the verge of collapse. The building of the berms increased shear stresses and confining pressures in the berms bringing the state of the soil very close to the CSB and further additions of the material in the berm brought the state of soil on to the CSB in an undrained manner. There was insufficient time for the dissipation of the pore pressures, which triggered the flow slides. Kramer and Seed (1988) observed that for a loose sand consolidated to K_O - conditions, only a small undrained increment of load is sufficient to trigger flow liquefaction. The tests by Kramer and Seed (1988) simulate the undrained failures in the Beaufort sea.

Physical Setting of the Fraser River Delta

The Fraser River delta front is fed by a network of active and relict distributory channels. The most conspicuous feature of the delta is a broad intertidal flat with a gradient of approximately 0.05 degrees, forming a platform approximately 5 to 10 km wide extending from the edge of the dykes to the break in slope at approximately 9 m below the lowest normal tide (Luternauer, 1980). Figure 4 shows a plan of the Fraser River Delta and shows that the lower part of the delta foreslope has an average gradient of approximately 1.5 degrees (Mathews and Shepard, 1962), but may be inclined as steeply as 23 degrees along its upper reaches (Scotton, 1977). The delta is in a seismically active region, but no local earthquakes were reported at the time of the large liquefaction submarine flow slide in 1985 (McKenna and Luternauer, 1987). Marine geophysical mapping has identified a number of slope instability events in recent sediments and has demonstrated that flow slides occurring in the river mouth incise deep debris flow channels into the delta foreslope (Christian et al, 1997).

The main channel of the Fraser River carries approximately 88% of the sediment-laden water discharged by the Fraser River into the Strait of Georgia (Mckenna et al., 1992). The snow melt freshet (May to July) carries 80% of the total sediment load. Over 50% of the sediment load is comprised of sand which is deposited at the mouth of the Main Channel at Sand Heads. The progradation rate of the delta at a depth of 9 m is approximately 9 m/year in the vicinity of the river mouth (Mathews and Shepard, 1962) and builds in thickness at about 12 cm/year (Barrie, pers.comm., 1994). The average sedimentation rate in the prodelta region is 2.16 cm/year (Moslow et al., 1991).

Northwest winds have the longest effective fetch (approximately 50 km) and consequently generate the highest waves (Thomson, 1981). Average wave height at the

delta front is about 0.6 m and maximum significant wave height is about 2.7 m during winter storms (Luternauer and Finn, 1983). Mean tidal range is 2.6 m with a maximum tidal range of 5.4 m.

Geophysical surveys show that the distributary mouth bar deposit at Sand Heads is incised by a series of deep gullies that coalesce downslope into a single large canyon (Kostaschuk et al., 1991, Hart et al., 1992). Heads of submarine canyons provide a favorable environment for slumping because of their steeper inclinations and their action as sediment traps (Morgenstern, 1967, Christian et al., 1997). The sea valley system has upslope tributary channels joining a single sinuous channel which splits into distributary channels at the base of the delta front (Kostaschuk et al., 1991). These distributary channels terminate in a submarine debris fan at the base of the slope. The tributary channel gradients vary from 23 degrees locally in the upper reaches of the tributaries at the river mouth to 2 degrees at 45 m depth. The major gullies were formed as a result of mass wasting events transforming to debris flows and are maintained by the sliding of accumulated gully bottom sediments and flushing action of tidal currents (Mathews and Shepard, 1962; Terzaghi, 1962; Scotton, 1977; Shepard and Milliman, 1978, Hart et al., 1992). Christian et al. (1997) concluded that the western margins of these debris canyons exhibited slopes in excess of 40 degrees which was attributed to undercutting and recurrent oversteepening by debris flows.

Five known major mass wasting events have occurred between 1970-1985 on the upper delta slopes at the mouth of the Main Channel of the Fraser River (McKenna et al., 1992). An investigation of the conditions leading to failure that occurred in 1985 is the objective of this paper. The following describes the evaluation of different triggering mechanisms responsible for this and other, similar events.

Steady State Characteristics of the Fraser River Delta Sand

Laboratory tests have been performed on FRD sand samples to establish steady state characteristics of the sand. Samples were prepared to different densities using both moist tamping methods and water pluviation techniques. Field tests including cone penetration tests (CPT) and seismic cone penetration tests (SCPT) have also been performed in the Delta . Laboratory and field test results are used to characterize the delta front sand deposits and are reported in a companion paper by Chillarige et al. (1997). A typical undrained triaxial compression stress path and a drained triaxial compression stress path of tests on FRD sand are shown in Figure 5. The undrained path in the e-p' plane remained horizontal without any changes in void ratio. The change in the void ratio can be seen in the drained path. The undrained stress path in the p'-q plane represents very brittle behavior and strain softening response of the sample to its steady state value at low stresses. The slope of the drained stress path in the p'-q plane is a straight line with a slope of 3:1. The ultimate points of the test paths for the FRD sand are on the steady state line. The slope of the collapse surface, 't' is determined as the slope of the line joining the peak shear stress to the steady state of the undrained stress path. The slope of the contractant state boundary surface (CSB), 's', can also be determined as the slope of a tangent drawn to the post peak portion of undrained stress path at steady state in the p'-q plane. From the laboratory test results, the steady state parameters are determined, following Sasitharan (1994), as

Γ = 1.11 (Ordinate of the steady state line at p' = 1 kPa in the e-ln p' plane)

λ_{ln} = 0.029 (Slope of the steady state line in the e-ln p' plane)

M = 1.4 (Angle of shearing resistance at steady state Φ' = 35^{o})

t = 0.8 (Slope of collapse surface in the p'-q plane)

s = 1.00 (Slope of contractant state boundary in the p'-q plane)

Evaluation of Sedimentation Effects

The shift in the position of the delta-front crest (10 m contour) was used as a base for reporting the liquefaction failures of the sediments in the FRD (McKenna et al., 1992). Figure 6 presents the bathymetric contours of the foreslope of the FRD in the area adjacent to Sand Heads and also shows the areal extent of the flow slide that occurred at 10 m depth between 27 June and 11 July 1985 (McKenna and Luternauer, 1987). The volume of the sediment involved in the flow slide is very extensive (greater than one million cubic meters). Bathymetric soundings at the area of the failure provided the post-event changes of the contours. Figure 7 shows the cross-section of the slope (Section 1-1 in Figure 6) obtained from the contours of the foreslope. The foreslope had a maximum angle of inclination of 23 degrees before the failure. The post-event head scarp had a relatively steep slope with vertical relief of about 15 m and intersects basal planes which are subparallel to the original seafloor, dipping at angles of about 6 degrees. The foreslope constitutes the extreme configuration of the slope before a liquefaction failure could occur. When flow liquefaction is initiated in the slope, the failure retrogresses towards its upper reaches, developing a flow slide. The retrogression continues until a stable or dense sand in the head scarp is encountered. The state of stress in the slope before failure brings the state of the sediments in the slope to the verge of collapse. To determine whether the slope becomes unstable, it is necessary to establish the state of stress in the slope and locate this state relative to the collapse surface/contractant state boundary in stress space. A correct stress analysis should be performed by finite element calculations incorporating a realistic constitutive model to describe the stress-strain behavior of the soil.

In the FRD, when slope failures occur in the fresh deposits of silty sands, the scar is replenished by the sediments of the Fraser River. Thus, in reality, the slope in the FRD is

built up in parallel layers by the sediments from the backscarp of a previous failure. It is realistic to use a model simulating the sequential construction of the slope for estimating the stress state in the slope. The deposition of sediments occurs with thin lenses of silty material in sands. Sand interbeds typically can be characterized as minute gravity-flow events, as drill hole samples invariably show silt inclusions within a clean sand matrix, separated by silty intervals corresponding to tidal sedimentation (couplets), as described by Christian et al. (1997). It can be precluded that no excess pore pressures exist in the thin lenses of silt. An incremental finite element stress analysis, duplicating the building of the slope while incorporating drained linear elastic effective stress parameters, would be useful in simulating deposition in the delta. A finite element based program SIGMA/W handles such analysis very well and has been used.

The slope was discretized into a number of finite elements. The boundary conditions are such that the displacements at the base were constrained in either direction and the displacement behind the backscarp of the failure line was laterally constrained. Robertson and Campanella (1983) presented a method of interpretation of CPT results for sands for estimating stiffness properties. Based on the CPT results of the fresh deposits in the FRD (Chillarige et al., 1994), the Young's Modulus has been estimated as 15 MPa. A Poisson's ratio of 0.3 and a K_O value of 0.43, that is, (1- sin ϕ'), are additional parameters used in the analysis. SIGMA/W simulates the process of accretion of the slope by the addition of finite elements in parallel layers to the backscarp of the prvious failure having the same properties. In the analysis, the stress file obtained from the preceding layer becomes the initial condition for the succeeding layer.

Stress path evaluation due to sedimentation

The stress state in the slope of the FRD before failure can be estimated from the extreme configuration of the slope. Figure 8 shows contours of effective vertical stress based on the finite element analysis with a vertical exaggeration of 10. The maximum values of the vertical effective stress along the final failure plane occurs at a depth of about 36 m (node 616). The stress path of the elements in the p'-q plane can be evaluated due to sediment deposition (accretion of the finite elements) by plotting the calculated effective confining stresses (p') and the corresponding deviatoric stresses (q) at Gaussian points of the finite element mesh, where $p' = J_1'/3$ and deviatoric stress $q = \tilde{A}(3J_2)$; in which J_1' is the first stress invariant, $(\sigma_1'+\sigma_2'+\sigma_3')$, and J_2 is the second stress invariant, $\frac{1}{\sqrt{6}}\sqrt{(\sigma_1-\sigma_2)^2+(\sigma_2-\sigma_3)^2+(\sigma_3-\sigma_1)^2}$. Figure 9 illustrates the stress path of the elements due to the sediment deposition. Small magnitudes of tensile stresses are observed at the surface of slope. All the stresses are determined for a K_O value of 0.43 and they appear to follow the K_O line in the stress space. It can be observed that the the shear stresses increase due to the building of the slope. Also shown in Figure 9 is the steady state line which has been established from laboratory tests on reconstituted samples of FRD sand.

The development of the high shear stresses within the slope is an important component that can explain the observed instability. However, to understand the potential for instability it is necessary to relate the in-situ stress state to that of the contractant state boundary (CSB), since instability will result when the in-situ stress state is moved to the CSB. Figure 9 shows all the stress states of the soil elements within the failure mass. However, it is difficult to compare all these stress states with the CSB since the CSB will change with soil density. To assist in the comparison between in-situ states and the relevant CSB, the stress path of the maximum shear stresses along the assumed failure

plane (from node 1800 to node 616) is shown in Figure 10b. Figure 10a shows the estimated in-situ state of the sand within the failure mass in terms of void ratio, e, and mean normal effective stress, p'. This estimated in-situ state was based on the in-situ shear wave velocity measurements (Chillarige et al., 1997). The estimated in-situ states in e-p' space are above the steady state line for the same Fraser River sand. This implies that the sand is very loose and could strain soften to steady state during undrained shear loading. Based on the estimated in-situ state, the steady state undrained shear strength is very small. At a depth of about 16 m on the failure plane (node 1800, Figure 8) the mean normal effective stress at steady state p'_{SS} will be about 10 kPa. At a depth of 36 m (node 616) p'_{SS} will be about 75 kpa. These values represent undrained shear strength ratio (s_u/σ_v') amounts of about 0.1, which are consistent with published back analysis values. Figure 10b shows the in-situ stress state of node 1800 to 616 compared to the different CSB's. It is clear from Figure 10b that the in-situ stress states of the sand along the assumed failure plane are very close to the estimated CSB. However, provided the sedimentation process is drained the stress state is marginally stable.

It appears that the sedimentation process develops high shear stresses within parts of the potential failure mass and the in-situ states are very close to the contractant state boundary (CSB). Hence, the freshly deposited sediments have a potential for flow liquefaction. However, the sedimentation process itself is unlikely to trigger instability. The following sections describe and evaluate the possible trigger mechanisms that could push the stress states onto the CSB and cause instability and flow.

Evaluation of Surface-wave Effects

The effect of surface waves in causing deep seated liquefaction flow slides in the FRD has been presented in detail by Chillarige et al., (1994). A theoretical investigation was

carried out to evaluate the effect of surface waves as a triggering mechanism and was also supported by a field investigation of in-situ porewater pressures for surface waves. Two probes were designed, constructed and installed to monitor pore pressures for the surface waves. Results from the field study suggested that the pore pressures were not significant enough to cause any deep seated failures. The theoretical investigation was based on the concept of threshold shear strain. Surface waves can cause both transient and residual pore pressures. The two types of pore pressures can be distinguished by the concept of the threshold shear strain. Residual pore pressures start building up when the shear strain associated with a wave exceeds a value of about 10^{-2}%. Wave conditions at the time of the 1985 failure were predicted using wind data and hindcasting. A maximum significant wave height of 2.7 m with a period of 5.32 sec and a wave length of 40 m was obtained. The shear strain associated with the maximum wave was calculated and observed to be less than the threshold shear strain. It was concluded that the surface waves in the Fraser River Delta cannot develop significant residual pore pressures. However, small magnitudes of transient pore pressures can be created by the waves in the deposits. The consequence of these small pore pressures is that the surface waves could only trigger instability of the sediments in the upper few meters of depth. This theoretical study was supported by field observations that wave induced pore pressures are significant only in the upper 2 to 3 m of sediments. Luternauer and Finn (1983) also concluded that wave loading could not initiate deep-seated failures in delta front sands.

Evaluation of Tidal Effects

It was believed that excess pore pressures in low permeability materials during low tides triggered liquefaction flow slides in Kitimat Fjord, Canada in 1975 (Johns et al., 1986). However, the influence of tidal drawdown on the stability of the sand deposits has not been quantified. Koppejan et al. (1948) and Terzaghi (1956) speculated that seepage

pressures during low tides were triggering flow liquefaction in submarine deposits. Seepage pressures are created during low tides due to the storage of pore water in the aquifers. Kramer (1988) assumed that flow liquefaction may be triggered in shoreline sand deposits for very small changes in shear stress under undrained conditions during low tides. He also identified that if the sand is in equilibrium initially under shear stresses higher than the steady state strength of the soil, the triggering of flow liquefaction may lead to flow sliding. However, this explanation lacks sufficient evidence since deep deposits will not experience shear stress changes due to tidal drawdown. Hence, the theory does not explain the initiation of flow liquefaction in deep deposits.

Gas generation is a natural phenomenon in river deltas. Organic material is deposited along with the river borne clastics in estuaries. Burial of some marine organisms may also occur during deposition. Consequent decay of the organics results primarily in methane gas generation. Methane gas is relatively insoluble in sea water and readily comes out of solution if total stress is reduced. Gas generation in occluded form in the pore water desaturates the sediments. It is also known that the effective stress state of sediments is very much influenced by the presence of gas in the sediments. The effect of tidal drawdown on gaseous sediments and its consequences on the liquefaction stability of sediments has not been studied in the past. The following section investigates the effect of tidal drawdown on both saturated sediments and unsaturated FRD sediments.

Tides are surface waves with long periods and impose periodic loading on the seabed. When tides propagate over a porous bed, such as a sand bed, water flows into and out of the porous medium. The phenomenon has been studied by several researchers as pore water pressure variations in the ground due to tide changes for a variety of boundary conditions (Ferris, 1951; Money, 1986; Pontin, 1986; Farrel, 1994). However, most of

these studies addressed the generation of pore pressures in the deposits due to tidal variations only in intertidal areas.

Tide loading can cause deformation of the seabed due to changes in total vertical stress. When the tidal wave length is large compared with the thickness of the permeable sea bed, the flow of water can be treated as a one-dimensional boundary value problem. The changes in pore water pressure are expressed in terms of the conservation principle applied to the mass of water in the pores of the sediment during its deformation. The net rate of flow of water expelled from an element of soil has to be equal to the net change of volume of the pores of the sediment. The modeling equation was given by Vuez and Rahal (1994) and can be expressed as

[1] $$\frac{1}{c_{vg}}\frac{\partial u}{\partial t}=\frac{\partial^2 u}{\partial z^2}+\frac{1}{c_v}\frac{\partial \sigma}{\partial t}$$

in which c_{vg} and c_v are the consolidation coefficients of gaseous sediments and saturated sediments respectively and are given by

[2,a] $$c_{vg}=\frac{k}{\gamma_w(n\beta+m_v)}$$ and

[2,b] $$c_v=\frac{k}{\gamma_w m_v}$$

where

k = coefficient of permeability of soil skeleton

n = porosity of the soil structure

β = compressibility of pore fluid

m_v = compressibility of soil skeleton

u = pore water pressure

σ = total stress due to tidal loading = $\frac{\gamma_w H}{2}\sin(\omega t)$,

in which, H is the tidal wave height and ω is the frequency

Equation 2,a includes the effect of the compressibility of pore fluid. Normally an increment of total stress on a soil is carried partly by the pore fluid as pore pressure and partly by the soil skeleton as effective stress, depending on their relative compressibilities. In saturated soils the compressibility of the soil skeleton is much greater than that of the pore water, and thus essentially all of a stress increment applied to a saturated soil is carried by the pore fluid. In partly saturated soil, a stress increment is shared by both the pore fluid and the soil skeleton.

Tidal drawdown on saturated sediments

In saturated soils, the compressibility of the pore fluid is negligible. Hence, the compressibility term, β, for the pore fluid is negligible in Equation 2,a. Therefore the consolidation equation due to tidal loading on saturated sediments is of the form;

[3] $$\frac{\partial u}{\partial t} = c_v \frac{\partial^2 u}{\partial z^2} + \frac{\partial \sigma}{\partial t}$$

Equation (3) describes the pore water pressure response for the propagation of tidal cycles over a saturated porous bed. The solution of the equation results in the variation of pore pressures in saturated sediments for tidal change in the FRD at the time of failure in 1985. Based on the Tide Tables, published by the Department of Fisheries and Oceans, Ottawa, Canada, the maximum tidal variations during the period of failure in 1985 were computed to be about 5 m with a period of about 16 hr . The time span of the tide from its peak to its low is about 8 hr. Actual field measurements of pore pressure response were made

over a month-long period, using a seabed monitoring array (Christian et al., 1997). These data were in agreement with predictions in the analysis described herein.

The solution of Equation 3 can be obtained using finite-difference methods. The tide-induced pore pressures are observed to be in phase with the tidal variation. The pore pressure response is a function of magnitude of tidal loading and permeability and compressibility characteristics of the porous medium. No residual pore pressures remain during low tide conditions. Hence, there are no changes in the effective stress conditions. The one-dimensional undrained analysis demonstrates that tidal drawdown cannot trigger flow liquefaction of deep saturated sand deposits at the mouth of the Main Channel of the Fraser River.

Tidal drawdown on gaseous sediments

It has been observed that gases expand and come out of solution in undisturbed samples of marine soils because of the release of the total stress. The presence of methane gas is quite common in marine soils, as a by-product of decomposition of organics. As gas is generated in the soils, the degree of saturation decreases. High concentrations of methane has been observed in pore fluid samples of the FRD (Christian et al., 1997). Esrig and Kirby (1977) have examined the relationship between the in-situ degree of saturation and the degree of saturation which would be measured in a sample at atmospheric pressure. Estimates of the degree of saturation in the samples showed lower values than those that must be present in the field. They also observed that the degrees of saturation in the field were always greater than 85%.

Fredlund and Rahardjo (1993) proposed that air bubbles are of spherical form in an occluded zone within the pore fluid (S = 100% -80%). The pore air and pore water pressures are assumed to be equal in the occluded zone. Hence, the normal definition of

the effective stress principle for saturated soils remains unchanged for soils with occluded air bubbles in the pore water. However, the presence of bubbles renders the pore fluid much more compressible than if the pore fluid were saturated.

Fredlund and Rahardjo (1993) state that the compressibility of an air-water mixture is predominantly influenced by the compressibility of the free air portion and also observe that the inclusion of even 1% air in the soil is sufficient to significantly increase the pore fluid compressibility. As the percentage of air increases to about 15% (S = 85%) the compressibility of the pore fluid can be as much as the compressibility of the soil skeleton. The presence of gas bubbles, such as methane, in pore water may change the compressibility of the gas-water mixture. However, it is assumed that the compressibility of pore air-water mixture and the compressibility of gas-water mixtures are of the same magnitudes. This assumption is reasonable because the isothermal compressibility of air/methane is equal to the inverse of the absolute air/methane pressure.

The mathematical model of the effect of tidal variations on gaseous sediments (Equation 1) requires the porosity of the soil skeleton and the compressibility of the pore fluid. It is estimated previously (Figure 11a) that the in-situ void ratio of the sand deposits in the failure zone is about 0.98 to 1.00. A lower bound value of 0.49 is used for porosity in the present analysis.

The in-situ degree of saturation in the marine sediments is now estimated to be between 85% to 100%, based on in-situ fluid/gas testing (Christian et al., 1997). However, no data regarding the in-situ degree of saturation is available for the time of the failure in 1985. Hence, it is reasonable to investigate the influence of pore fluid compressibilities on the response of sediments for tidal variations over the range of degree of saturation (100% - 85%). It was demonstrated that low tides can not initiate flow liquefaction

failures in saturated sediments. Hence, the analysis can be carried out at different degrees of saturation (99% - 85%). However, small percentages of gas may go into solution in the pore fluid during flood tide. When the gas dissolves in the solution, the pore fluid can be treated as fully saturated. Hence, the present analysis considers the degrees of saturation of the sediments between 98% to 85%.

Table 1 presents the values of different pore fluid compressibilities over the range of degrees of saturation, obtained from the analysis done by Fredlund and Rahardjo, (1993). For fully saturated sediments (S = 100%), the compressibility of pore fluid is negligible. However, the compressibility of pore fluid for the degrees of saturation between 98% to 85% is considerable relative to the compressibility of the FRD sand skeleton, which is obtained from the laboratory testing of the sand samples.

Equation 1 describes the pore fluid response in gaseous sediments for tidal loading. As previously discussed, the maximum tidal variation at the time of the flow slide in the FRD was about 5 m with a period of 16 hr. The pore fluid response is obtained using finite difference methods for a degree of saturation of 98%. Figure 11 presents the response of the pore fluid with a gas of 2% for a depth of 36 m. It can be observed that the tide-induced pore pressures are out of phase by about 1 hr 25 min. in gaseous sediments. A residual pore pressure of about 13 kPa can be observed at low tide. Hence, a partially drained condition prevails in the sediments during low tide. The amplitude change of pore pressure is about 30% of the total stress variation. Thus, the effective stress conditions change in the sediments due to tidal variation. During low tide conditions, gas tries to expand and thus increases the pore pressures.

The recent deposits in the FRD have degrees of saturation ranging between 85% to 100%. The influence of the saturation can be observed in the excess pore pressures that exist

during low tide conditions. Over this range of saturation, the magnitude of the excess pore pressures increase with a decrease of degree of saturation. The smaller the degree of saturation the greater the time lag. However, the variation of the excess pore pressures with the decrease in saturation is not pronounced. For the tide of 5 m with a period of 16 hr, excess pore pressures of about 13 kPa and 17 kPa are observed at low tide conditions for 98% and 85% saturation, respectively. This is because the compressibility ratio (r) of soil skeleton and pore fluid does not change significantly at lower degrees of saturation (Table 1). Hence, a stress path evaluation for the changes in pore pressures at S = 98% is reasonably valid to embody the effect of different degrees of saturation.

Stress path evaluation due to tidal drawdown on gaseous sediments

As discussed previously, the in-situ stress states are close to the CSB before the 1985 failure occurred. The effect of the tidal variation is examined on the in-situ stress state of sediments at a depth of 36 m (node 616) and is presented in the Figure 12. The stress path (Figure 12b) shows that the shear stress is essentially unchanged during the tidal drawdown. Tidal variation will not apply any additional shear stresses on the sediments. From Figure 11, it was observed that the pore pressures are partially dissipated during the rise of the tide. This indicates that the mean effective stress, p', increases with the rising tide as shown in Figure 12b. The mean confining stress increases from a value of 220 kPa to 236 kPa. Figure 11 also shows that residual pore pressures remain as the tide recedes to its low value. The stress path during this phase (Figure 12b) shows that the mean confining stress decreases from the value of 236 kPa to about 200 kPa with a constant shear stress value. At the extreme low tide stage, the mean confining stress reaches its lowest value along the constant shear stress path.

During the partial dissipation of pore pressures, volume changes also occur in the sediments, that is, changes in void ratio occur due to tidal variation on the gaseous sediments (Figure 12a). It was determined previously that the void ratio of the stress state of the sediments in the FRD at a depth of 36 m is about 0.98. During the increasing tide, the increase in effective stress of the sediments represents a slight decrease in the void ratio that is, a small amount of consolidation occurs in the sediments. During the decreasing tide, the change in the void ratio indicates that the void ratio increases by a small amount. However, the change in the void ratio is very small since, the loading and unloading cycles are essentially elastic and do not exceed the threshold strain. Therefore, no soil hardening is expected.

As presented previously, any attempt to cross the CSB can result in collapse of the soil structure of the sediments and lead to rapid generation of pore pressures causing flow liquefaction. The observed stress path from the tidal variation of 5 m on the gaseous sediments (S = 98%) is in the constant shear stress plane. During low tide conditions, the gas expands slightly and the stress path can reach the CSB during this phase and attempt to cross the boundary. Structural collapse of the sediments can then occur. Consequently, the sediments can fail in an undrained manner. Figure 13 shows the CSB defined for an undrained test at a void ratio of 1.0. The calculated stress path at a depth of 36 m clearly reaches the CSB at the extreme low tide conditions and eventually, the sediments can experience flow liquefaction. Thus, the specific stress path explains the triggering of flow liquefaction at an extreme low tide.

Development of Flow Slides

It has been observed that the state of the fresh deposits of the FRD have a potential for flow liquefaction. The triggering of liquefaction of gaseous sediments at the in-situ stress

state during low tides can cause the development of an initial flow slide in the sediments. The loss in shear strength in the liquefied material can result in an initial flow slide. A model developed by Gu et al. (1993) describes the development of flow slides. The initial flow slide removes support for the remaining contractant gaseous sediments. These sediments will also be experiencing partially drained residual pore pressures during low tides. However, these pore pressures may not be sufficient to bring the state of the sediments on to the CSB. An undrained stress redistribution, as presented by Gu et al. (1993), can cause strain softening of the remaining unsupported sediments, which results in another flow slide. Progressive failure of the deposits, thus, continues generating a retrogressive flow slide. The slides cease to progress when a dense state of deposits or a stable back scarp is encountered. The mechanism explaining the triggering of flow liquefaction is consistent with the occurrence of retrogressive flow slides in river deltas during low tides.

Additional Mechanisms

Currents associated with tides and dredging are also believed to contribute to the initiation of flow liquefaction of the sediments. Erosion due to currents may cause local over steepening resulting in undrained local failures. Hence, it is not thought to be a contributing mechanism for a major failure, but may be the mechanism producing numerous small gravity flows observed in soil investigations at Sand Heads (Christian et al., 1997). Uncontrolled dredging operations may also induce local oversteepening in the sediments. Therefore, this may also lead to local undrained failures at shallow depths. Dynamic loading from ship's propellers may also initiate shallow flow slides.

The environmental conditions in the FRD suggest that the failure could have occurred on 2 July, 1985 when there was an extreme tide variation of about 5 m. The environmental

processes, such as sedimentation, low tide conditions and gas in the sediments, contributed to the failure. This conclusion is based on the assumption that the sediments in the delta had degrees of saturation between 98% to 85%. Samples of pore fluid in the Fraser River Delta have shown the presence of gas in the sediments.

Conclusions

Liquefaction flow slides are quite common in active river deltas and fjords. The flow slides are caused by triggering of flow liquefaction in loose sandy soils. These flow slides can be triggered either by dynamic loading or by static loading. In the Fraser River Delta, the occurrence of flow slides appears to be spread over the whole year. An analysis investigating the contributions of different environmental processes for a liquefaction flow slide that occurred in 1985 in the FRD has been carried out. An evaluation of sedimentation in the delta as a triggering mechanism shows that sedimentation may not initiate flow liquefaction failures, but it can develop high shear stresses that can bring the in-situ stress state of the sediments close to the collapse surface. Surface waves in the FRD cannot initiate deep seated flow failures, however, they can trigger shallow instability. An investigation of the effect of tidal drawdown on saturated sediments shows that the effective stress state of sediments remains unchanged and tidal drawdown cannot trigger flow liquefaction of the saturated sediments. However, gas generation within the sediments of the FRD induces desaturation in the sediments. The effect of tidal drawdown on gaseous sediments reveals that there will be residual pore water pressures in the sediments during low tide conditions and can lead to triggering of flow liquefaction failures during extreme low tide conditions. Progressive failure of sediments can develop retrogressive flow slides. Currents and dredging operations may also initiate local instability. The conclusions derived from the analysis may be used for explaining liquefaction flow slides in other river deltas.

Acknowledgement

The first author gratefully acknowledges financial support by the Canadian Commonwealth Scholarship Plan. Much of the field work was carried out by ConeTec Investigations Ltd. under contract to the Geological Survey of Canada. Discussions and valuable comments by Dr. D.C. Sego, Dr. P. Steffler and Dr. T.F. Moslow are also acknowledged. Encouragement by Dr. D.B. Prior is highly appreciated.

References

Alarcon-Guzman, A., Leonards., G. A., and Chameau, J. L. 1988. Undrained monotonic and cyclic strength of sands. Journal of Geotechnical Engineering, ASCE, **114**: 1089-1109.

Barrie, 1996. Personal communication.

Been, K., Jefferies, M. G., and Hachey, J., 1991. The critical state of sands. Geotechnique, **41**: 365-381.

Casagrande, A., 1936. Characteristics of cohesionless soils affecting the stability of earthfills. Journal of the Boston Society of Civil Engineers, **23**: 257-276.

Castro, G., 1969. Liquefaction of sands. Harvard Soil Mechanics Series No. 81, Harvard University, Cambridge.

Castro, G. and Poulos, S. J., 1977. Factors affecting liquefaction and cyclic mobility. Journal of Geotechnical Engineering, ASCE, **103**: 501-516.

Chillarige, A.V., Robertson, P.K., Morgenstern, N.R., Christian, H.A., 1997. Evaluation of in-situ state of Fraser River sand. Canadian Geotechnical Journal (companion paper submitted for review).

Chillarige, A.V., Robertson, P.K., Morgenstern, N.R., Christian, H.A. and Woeller, D.J., 1994. Evlauation of wave effects on seabed instability in the Fraser River Delta., Proceedings, 47th Canadian Geotechnical Conference, Halifax, 186a-186g.

Christian, H.A, Woeller, D.J., Robertson, P.K. and Courtney, R.C., 1997. Site Investigations to evaluate flow liquefaction slides at Sand Heads, Fraser River delta. Accepted for publication, Canadian Geotechnical Journal.

Dawson, R.F., Morgenstern, N.R. and Gu, W.H., 1992. Instability mechanisms initiating flow failures in mountainous mine waste dumps. Study for Energy, Mines and Resources, Canada.

Eckersley, J., 1990. Instrumented laboratory flow slides. Geotechnique, **40:** 489-502.

Esrig, M.I. and Kirby, R.C., 1977. Implications of gas content for predicting the stability of submarine slopes. Marine Geotechnology, **2**: 81-100.

Farrel, E.R., 1994. Analysis of groundwater flow through leaky marine retaining structures. Geotechnique, **44**: 255-263.

Ferris, J.G. 1951. Cyclic water level fluctuations as a basis for determining aquifer transmissivity. International Association of Hydrological Sciences, **2**: 148-155.

Fredlund, D.G. and Rahardjo, H, 1993. *Soil Mechanics for Unsaturated Soils.* John Wiley & Sons Inc.

Gu, W.H., Morgenstern, N.R. and Robertson, R.K., 1993. Progressive failure of the lower San Fernando dam. Journal of the Geotechnical Engineering Division, ASCE **119**: 333-348.

Hart, B.S, Prior, D.B, Barrie, J.V., Currie, R.G. and Luternauer, J.L., 1992. A river mouth submarine channel and failure complex, Fraser River Delta, Canada. Sedimentary Geology, **81**: 73- 87.

Ishihara, K., 1993. Liquefaction and flow failure during earthquakes. Geotechnique, **43**: 349-416.

Ishihara, K., Verdugo, R. and Acacio, A.A., 1991. Characterization of cyclic behavior of sand and post-seismic stability analysis. Proceedings, 9th Asian Regional Conference on Soil Mechanics and Foundation Engineering, Bangkok, Thailand, Vol. .2, pp. 17-40.

Johns, M.W., Prior, D.B., Bornhold, B.D., Coleman, J.M. and Bryant, W.R., 1986. Geotechnical aspects of a submarine slope failure, Kitimat fjord, British Columbia. Marine Geotechnology, **6**: 243-279.

Kramer, S.L., 1988. Triggering liquefaction flow slides in coastal soil deposits. Engineering Geology, **26**: 17-31.

Kramer, S.L. and Seed, H.B., 1988. Initiation of soil liquefaction under static loading conditions. Journal of Geotechnical Engineering, ASCE, **114**: 412-430.

Koppejan, A.W., Van Wamelan, B.M., and Weinberg, L.J.H., 1948. Coastal flow slides in the Dutch province of Zeeland. Proceedings of the Second International Conference on Soil Mechanics and Foundation Engineering, Rotterdam, Vol. 5, pp. 89-96.

Kostaschuk, R.A., Luternauer, J.L., Mckenna, G.T. and Moslow., T.F., 1991. Sediment transport in a submarine channel system: Fraser River Delta, Canada. Journal of Sedimentary Petrology, **62**: 273-282.

Lade, P.V., 1993. Initiation of static instability in the submarine Nerlerk berms. Canadian Geotechnical Journal, **30**.

Luternauer, J.L, 1980. "Genesis of morphological features on the western delta front of the Fraser River, British Columbia" - Status of Knowledge in *the Coast Line of Canada*, edited by McCann S.B., Geological Survey of Canada, Paper 80, pp. 381-396.

Luternauer, J.L. and Finn, W.D.L., 1983. Stability of the Fraser River Delta front. Canadian Geotechnical Journal, **20**: 603-616.

Mathews, W.H. and Shepard, F.P., 1962. Sedimentation of Fraser River delta, British Columbia. American Association of petroleum Geology, Bulletin 46, pp. 1416-1438.

McKenna, G.T. and Luternauer, J.L., 1987. First documented failure at the Fraser River Delta front, British Columbia. In *Current Research* , Part A, Geological Survey of Canada, Paper 87 - 1A , pp. 919-924.

McKenna, G.T. Luternauer, J.L. and Kostaschuk, R.A., 1992. Large-Scale mass wasting events on the Fraser River Delta front near Sand Heads, British Columbia. Canadian Geotechnical Journal, **29**: 151 -156.

Money, M.S. 1986. Tidal variations of groundwater level in an esturine aquifer. in *Groundwater in engineering geology, Edited* by Cripps, J.C., Bell, G. and Culashaw, G., Geological Society, Engineering Geology Special Publication, No.3, pp. 81-85.

Morgenstern, N.R., 1967. Submarine slumping and the initiation of turbidity currents. *Marine Geotechnique*, Edited by A.F.Richards, Urbana, Illinois, University of Illinois Press, pp. 189-210.

Moslow, T.F., Luternauer, J.L., and Kostaschuk, R.A., 1991. Patterns and rates of sedimentation on the Fraser River delta slope, British Columbia. in Current Research, Part E, Geological Survey of Canada, Paper 91- 1E, pp. 141 -145.

Pontin, J.M.A., 1986. Predictions of groundwater pressures and uplift below excavations in tidal limits. in *Groundwater in engineering geology, Edited* by Cripps, J.C., Bell, G. and Culashaw, G., Geological Society, Engineering Geology Special Publication, No. 3, pp. 353-366.

Poulos, S.J., 1981. The Steady state of deformation. Journal of Geotechnical Engineering Division, ASCE, Vol. **107**: 553-562.

Robertson, P.K., 1994. Suggested Terminology for liquefaction: An internal CANLEX report. University of Alberta, Alberta, Canada. pp. 1-20.

Robertson, P.K, and Campanella, R.G. 1983. Interpretation of cone penetration tests. Part I: Sand. Canadian Geotechnical Journal, **20** : 718-733.

Sasitharan, S. 1994. Collapse behaviour of very loose sand. Ph.D. thesis, Department of Civil Engineering, University of Alberta, Edmonton.

Sasitharan, S., Robertson, P.K., Sego, D.C. and Morgenstern, N.R., 1993. Collapse behavior of sand. Canadian Geotechnical Journal, **30**: 569-577.

Scotton, S. 1977. *The outer banks of the Fraser River Delta, engineering properties and stability considerations.* M.sc. Thesis, Department of Civil Engineering, University of British Columbia, Vancouver.

Shepard, F.P., and Milliman, J.D. 1978. Sea-floor currents on the foreset slope of the Fraser River delta, British Columbia (Canada). Marine Geology, **28**: 245-251.

Skopek, P., Morgenstern, N.R., Robertson, P.K. and Sego, D.C., 1993. Collapse of dry sand. Canadian Geotechnical Journal.

Sladen, J.A., D'Hollander, R.D. and Krahn, J., 1985a. The Liquefaction of sands - a collapse surface approach. Canadian Geotechnical Journal, **22**: 564-578.

Sladen, J.A., D' Hollander, R.D., and Krahn, J., 1985b. Back analysis of the Nerlerk Berm liquefaction slides. Canadian Geotechnical Journal, **22**: 579-588.

Terzaghi, K, 1956. Varieties of submarine slope failures. Proceedings, 8th Texas Conference on Soils and Foundation Engineering., University of Texas, Austin, pp. 1-41.

Terzaghi, K., 1962. Discussion of " Sedimentation of Fraser River Delta, British Columbia." by Mathwes and Shepard, 1962. American Association of Petroleum Geology Bulletin ,Vol. **46**: 1438-1443.

Thomson, K., 1981. *Oceanography of the British Columbia Coast*, Canadian Specialty Publication of Fisheries and Aquatic Sciences, 56, 291 p.

Vuez, A. and Rahal, A., 1994. Cyclic loading for the measuring of soil consolidation parameters. Proceedings, Settlement'94, Texas A&M University, College Station, pp. 762-774.

Permeability of deposits (m/sec)	1.44×10^{-4}				
Compressibility of FRD sand (m_v) (1/kPa)	1.3×10^{-4} (obtained from laboratory tests on FRD sand)				
Degree of saturation, S (%)	100	98	95	90	85
Compressibility of pore fluid (β) (1/kPa)	4.58×10^{-7}	4.5×10^{-4}	5.63×10^{-4}	7.3×10^{-4}	8.44×10^{-4}
Consolidation coefficient of gaseous sediments (c_{vg})	0.11	4.11×10^{-2}	3.55×10^{-2}	2.95×10^{-2}	2.65×10^{-2}
Ratio of compressibilities ($r = c_{vg}/c_v = m_v/(n\beta+m_v)$	1	0.37	0.32	0.27	0.24

Table 1. Compressibilities of pore fluid at different degrees of saturation and ratio of compressibilities of gaseous sediments to the saturated sediments

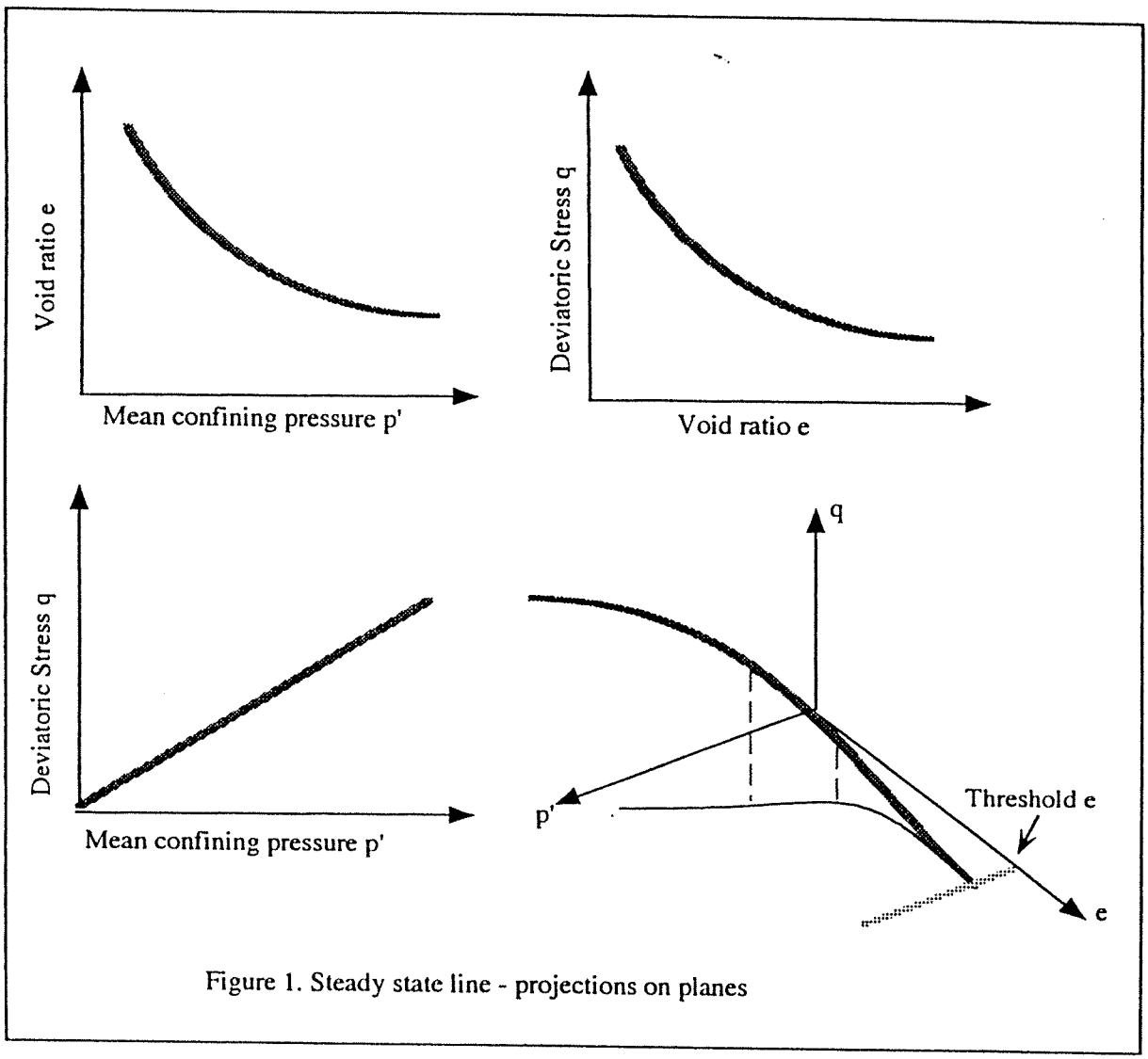

Figure 1. Steady state line - projections on planes

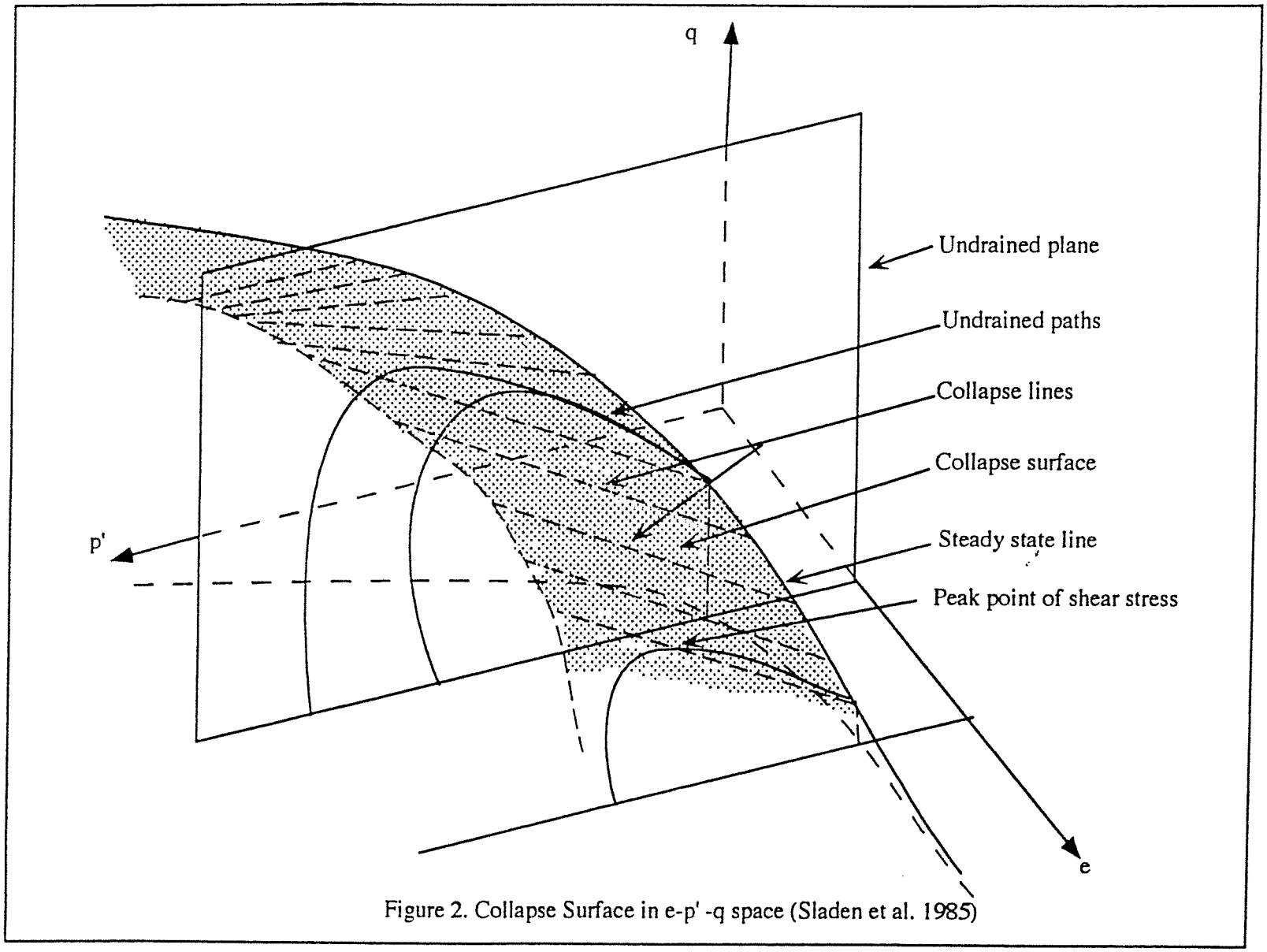

Figure 2. Collapse Surface in e-p' -q space (Sladen et al. 1985)

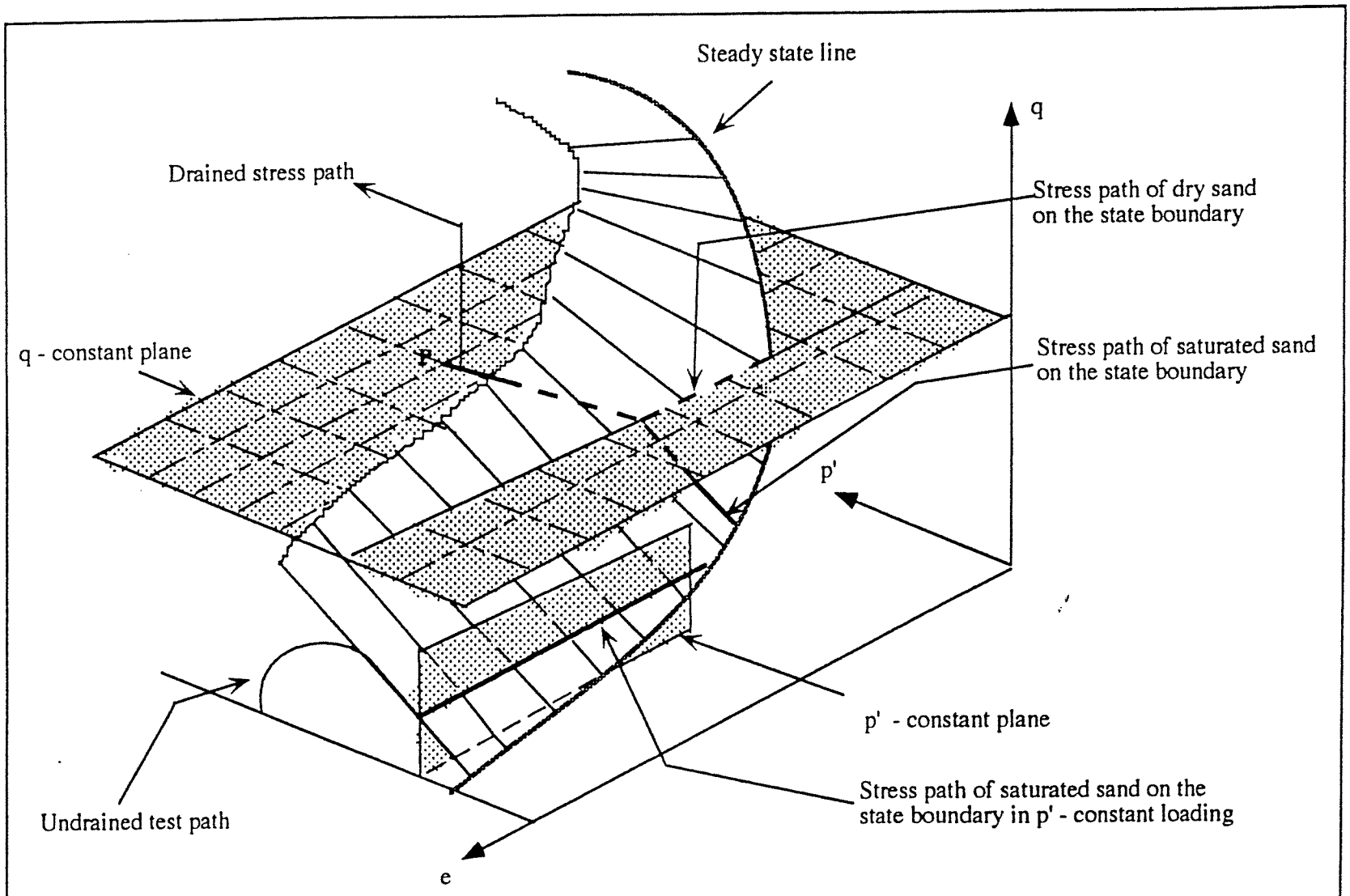

Figure 3. Confirmation tests for Contractant state boundary surface

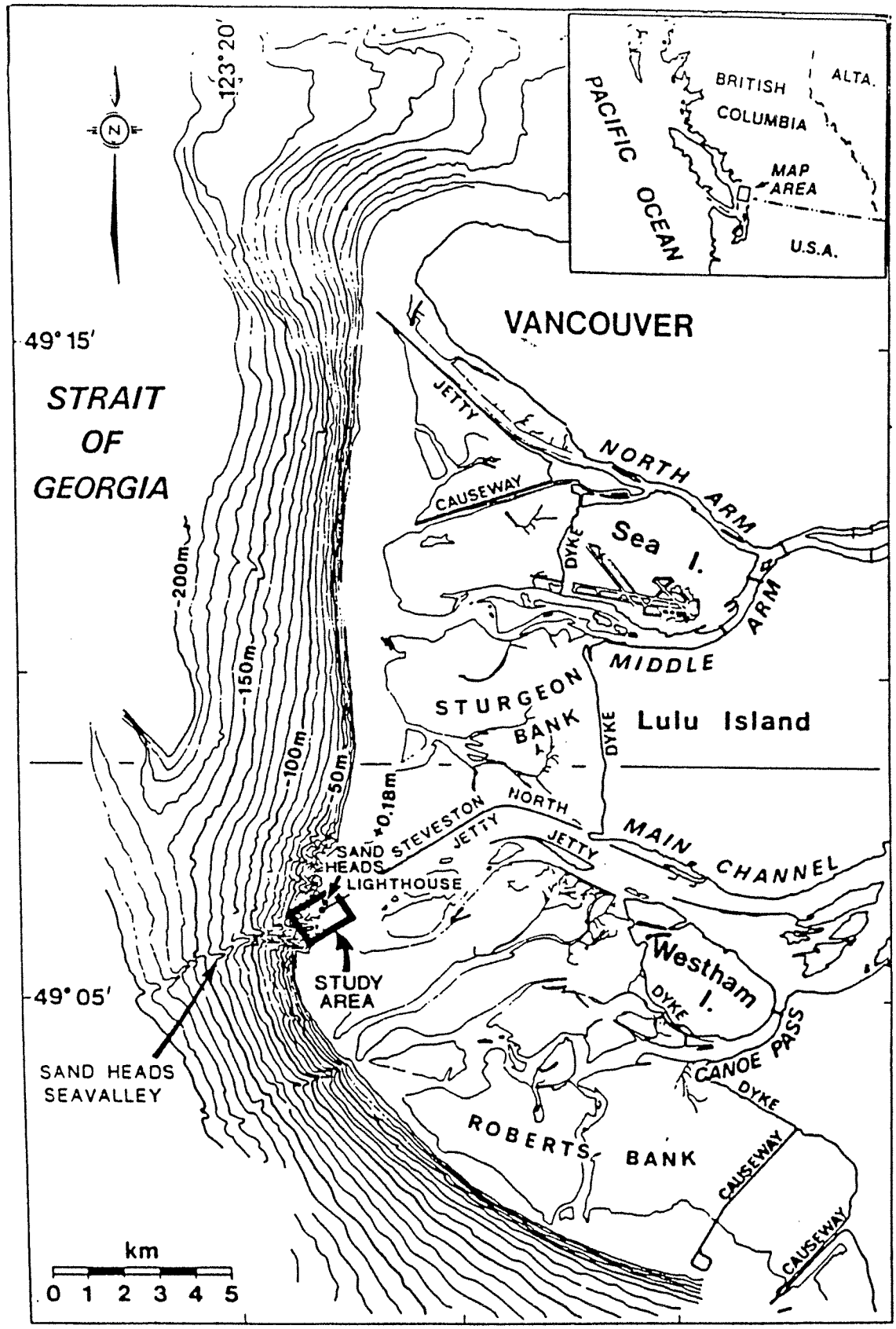

Figure 4. The Fraser River Delta front (after McKenna et al., 1992)

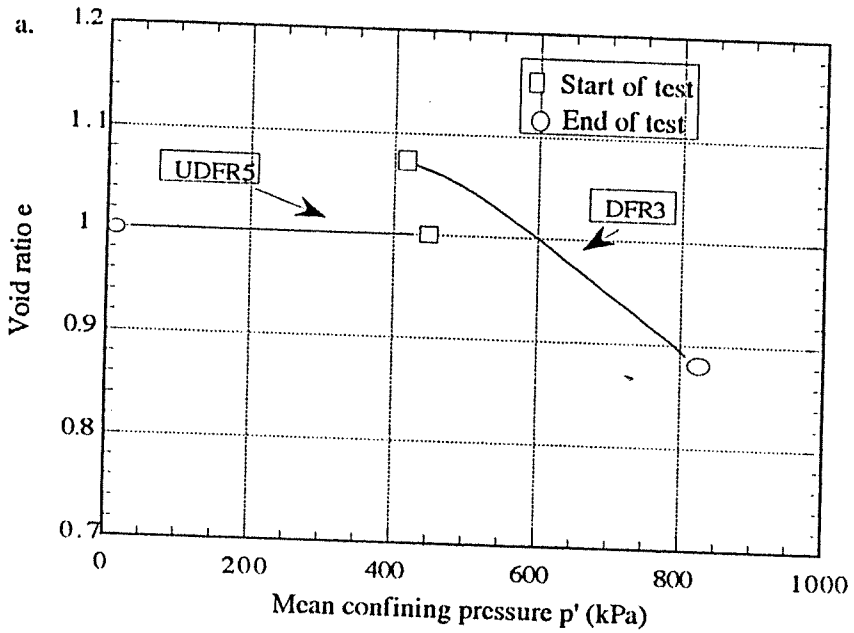

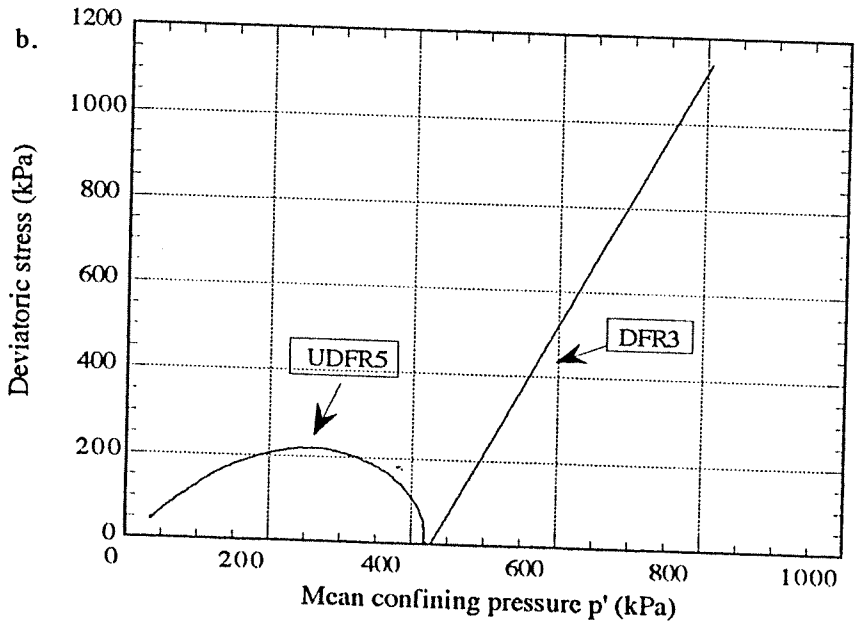

Figure 5. Typical undrained and drained stress paths

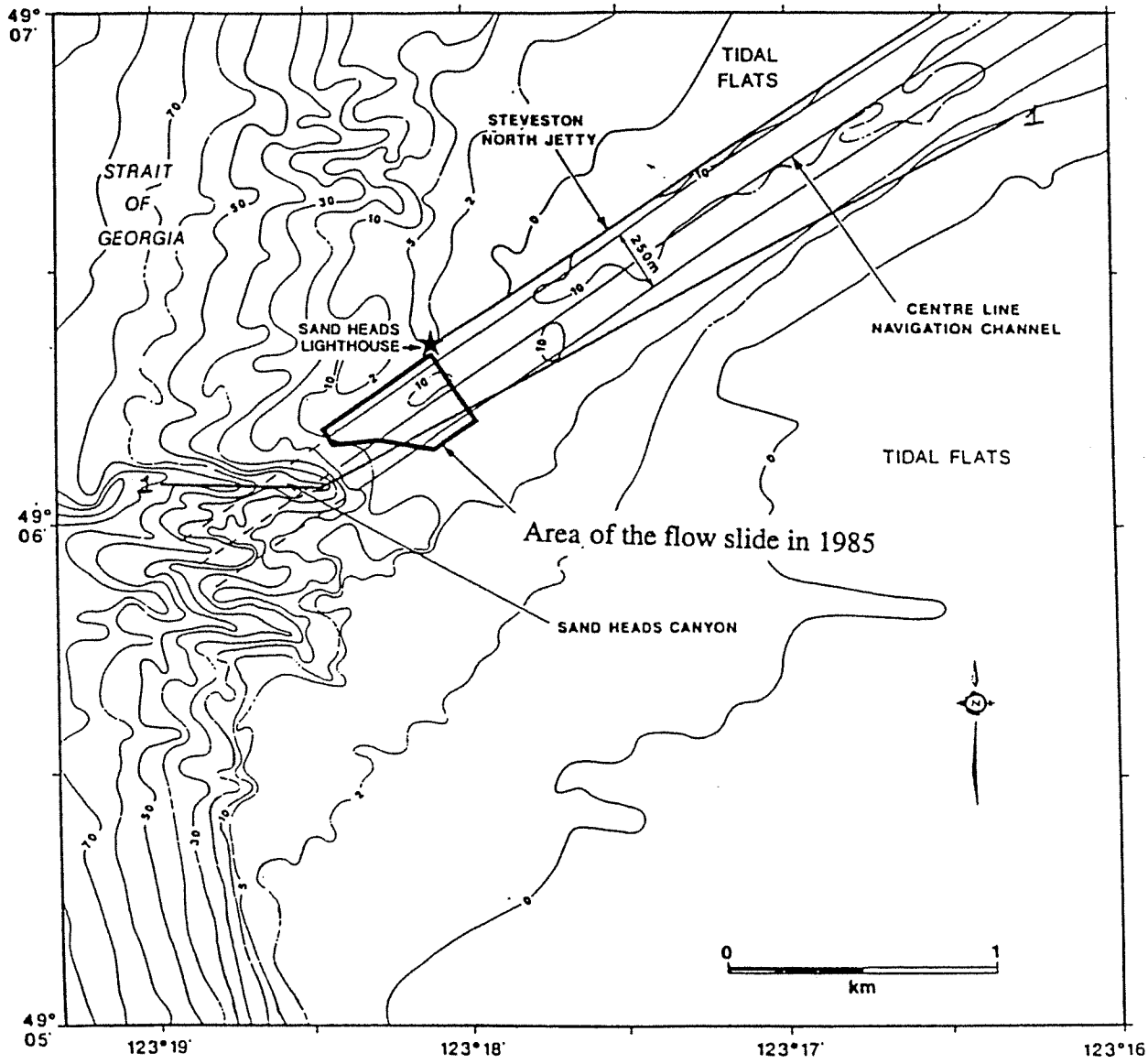

Figure 6. Morphology of the Fraser River Delta foreslope off the Main Channel (after McKenna and Luternauer, 1987). Box indicates the area of the flow slide in 1985

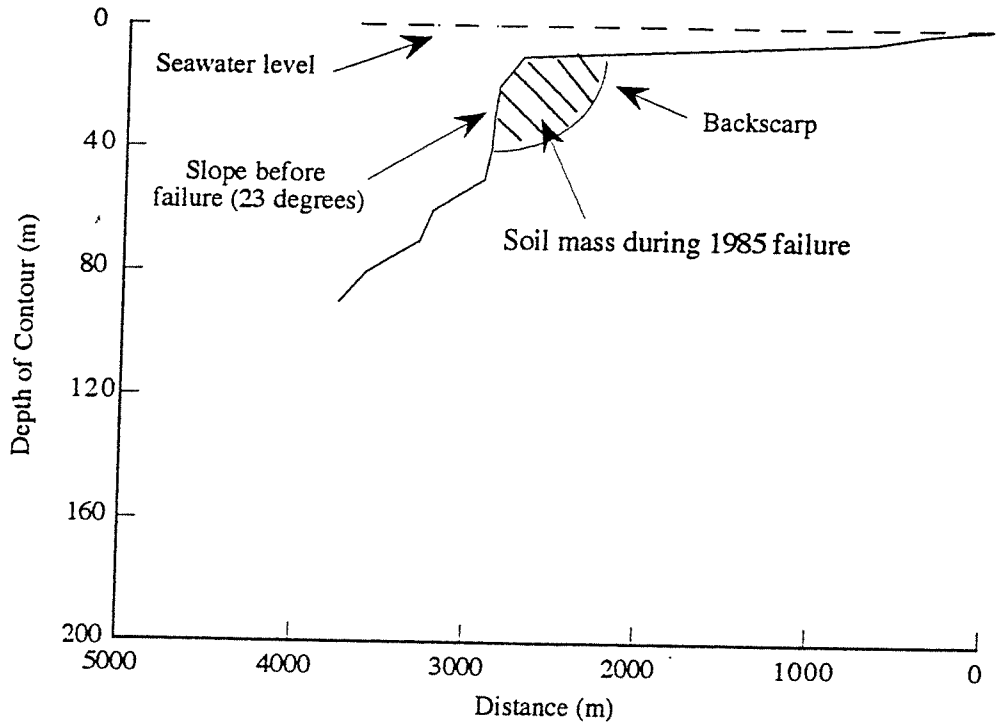

Figure 7. Slope along section 1-1 of Figure 6

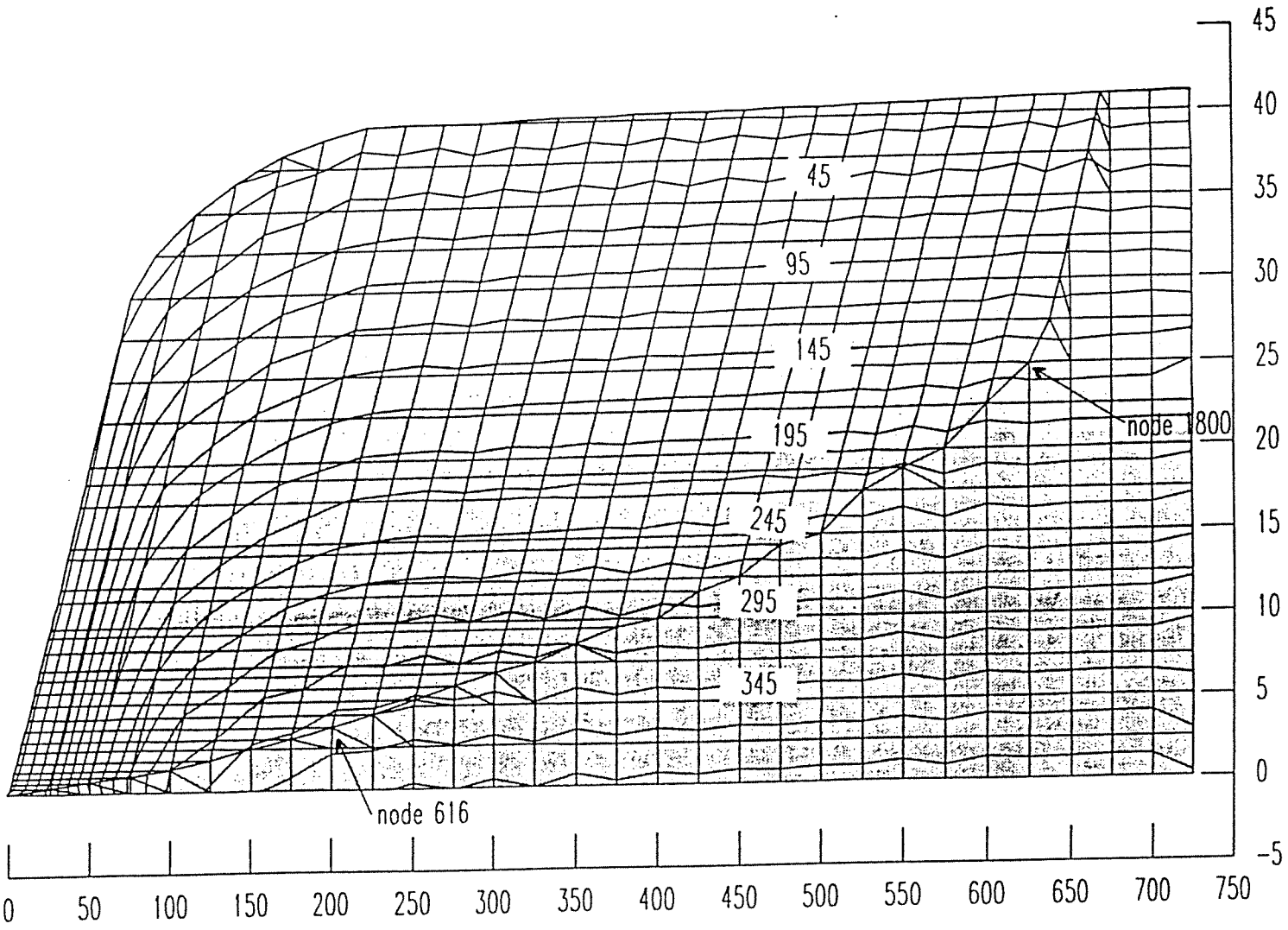

Figure 8. Contours of effective vertical normal stress

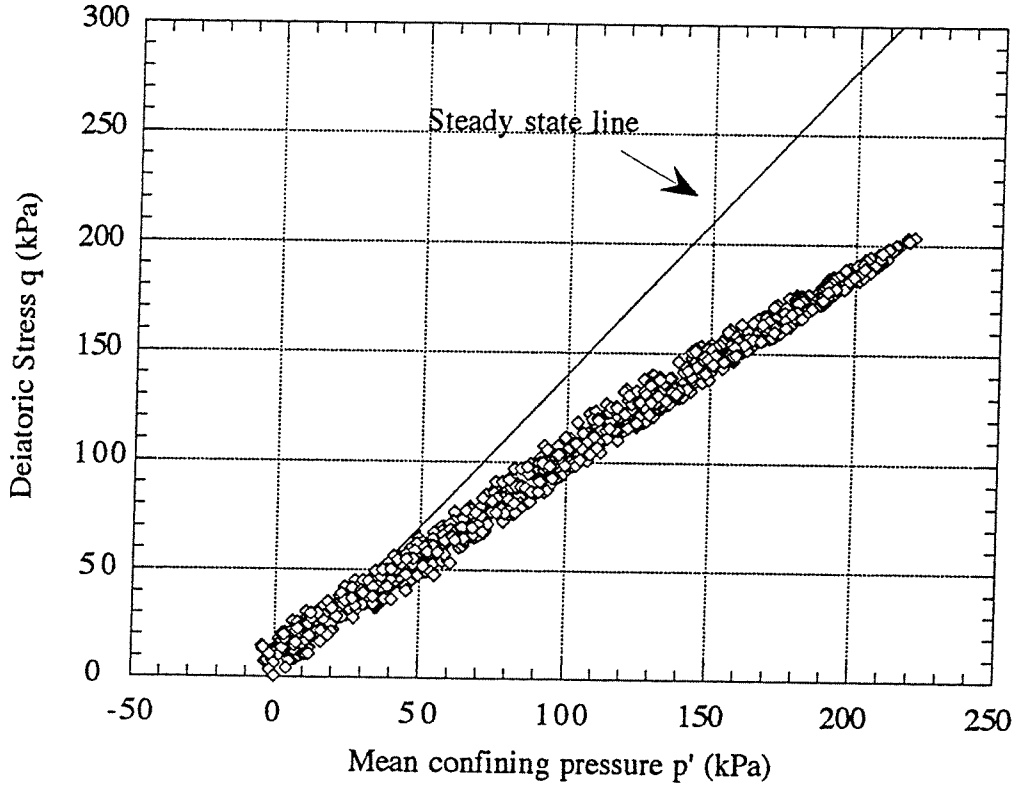

Figure 9. Effective stress state of elements in the slope

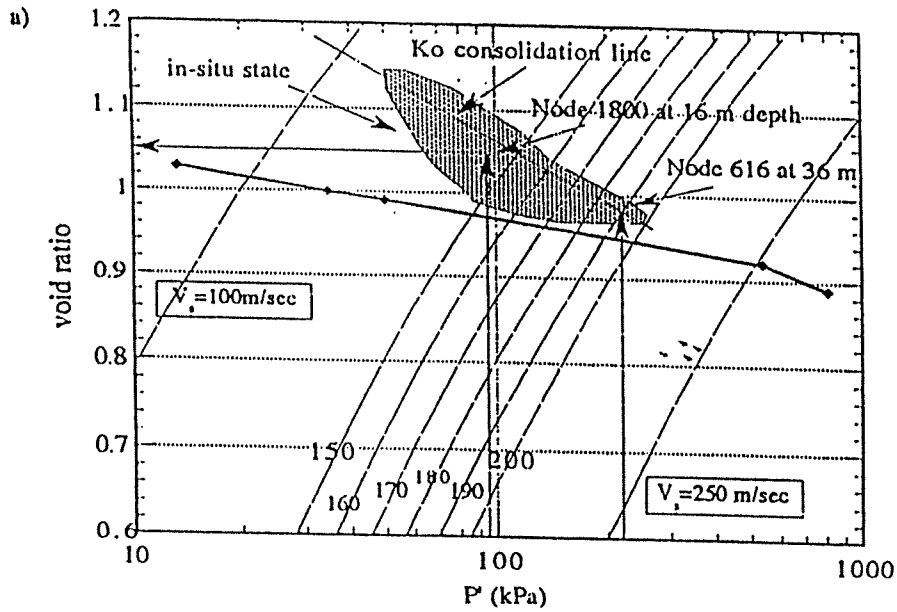

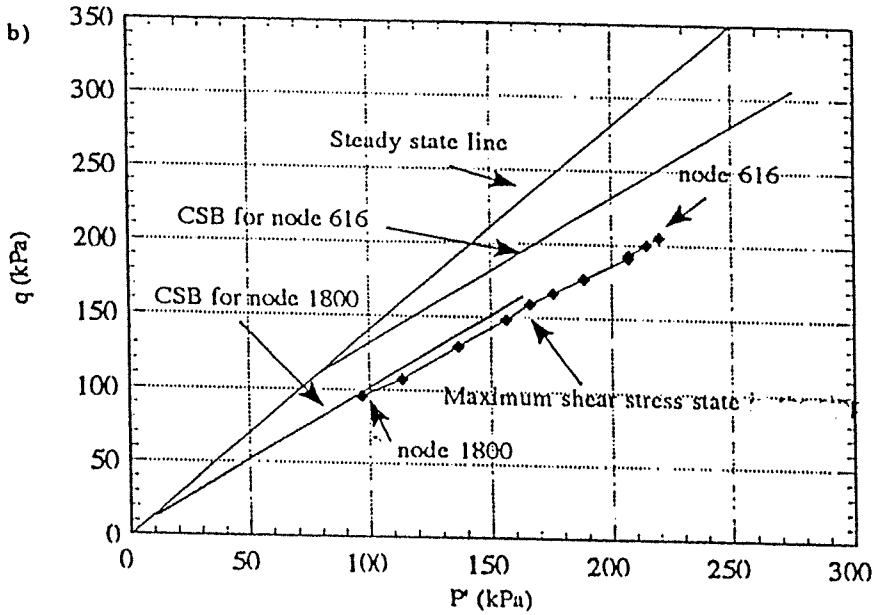

Figure 10. Characterization of the stress state in the fresh deposits of the FRD

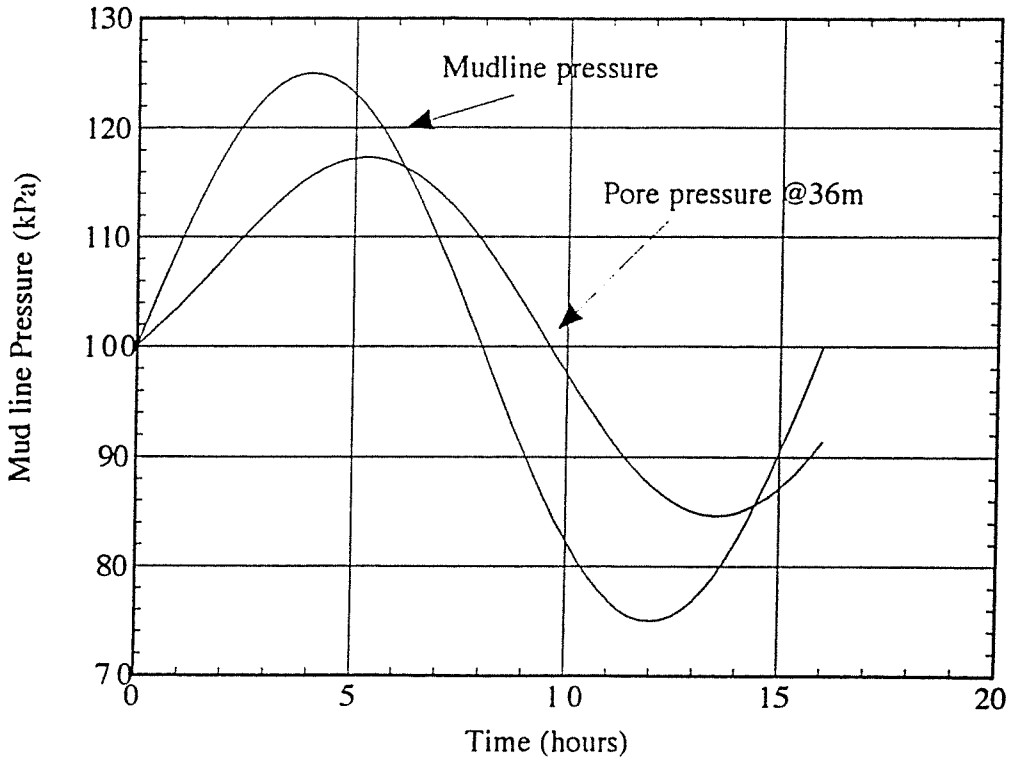

Figure 11. Variation of pressures for a tide of 5m with 16 hr period (S = 98%)

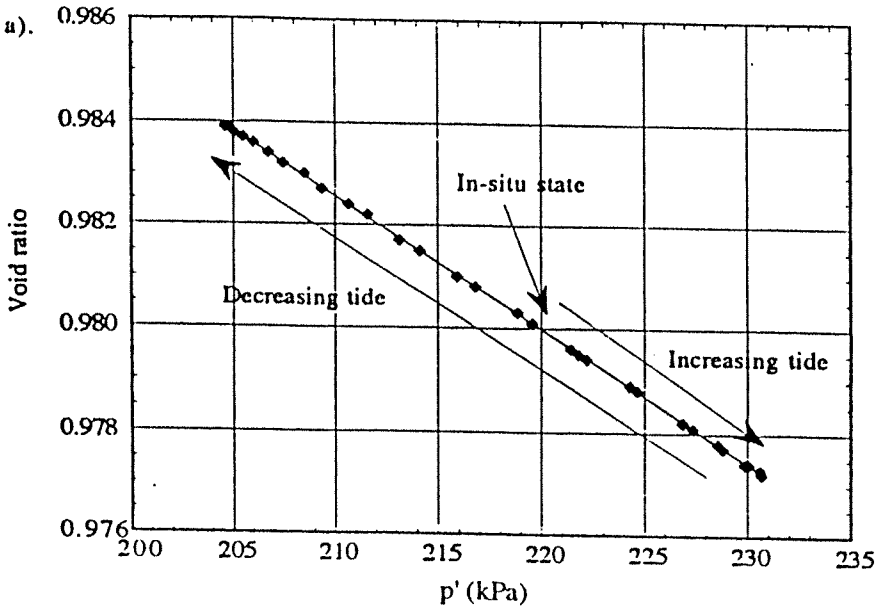

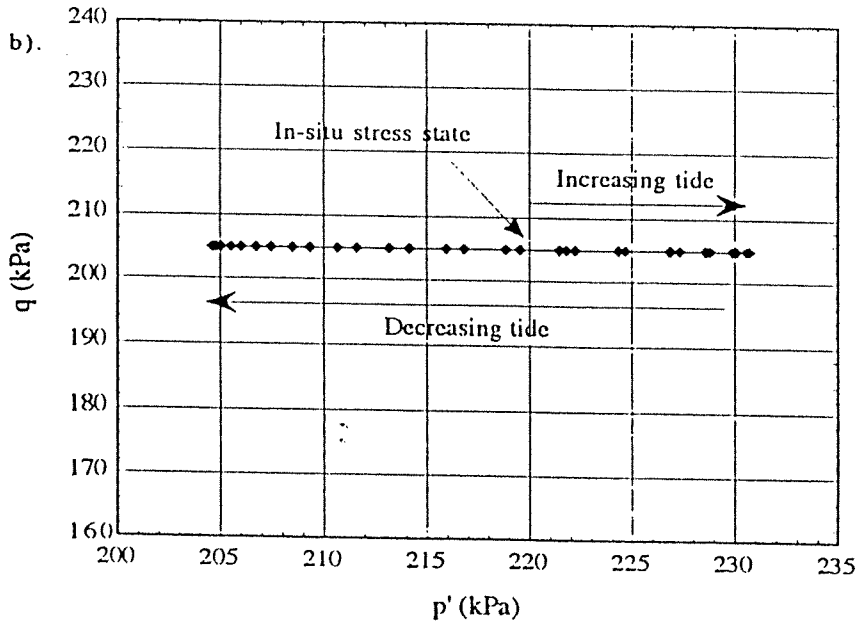

Figure 12. Stress path due to a tide of 5 m (when S=98%)
a). e-p' plane b). p'-q plane

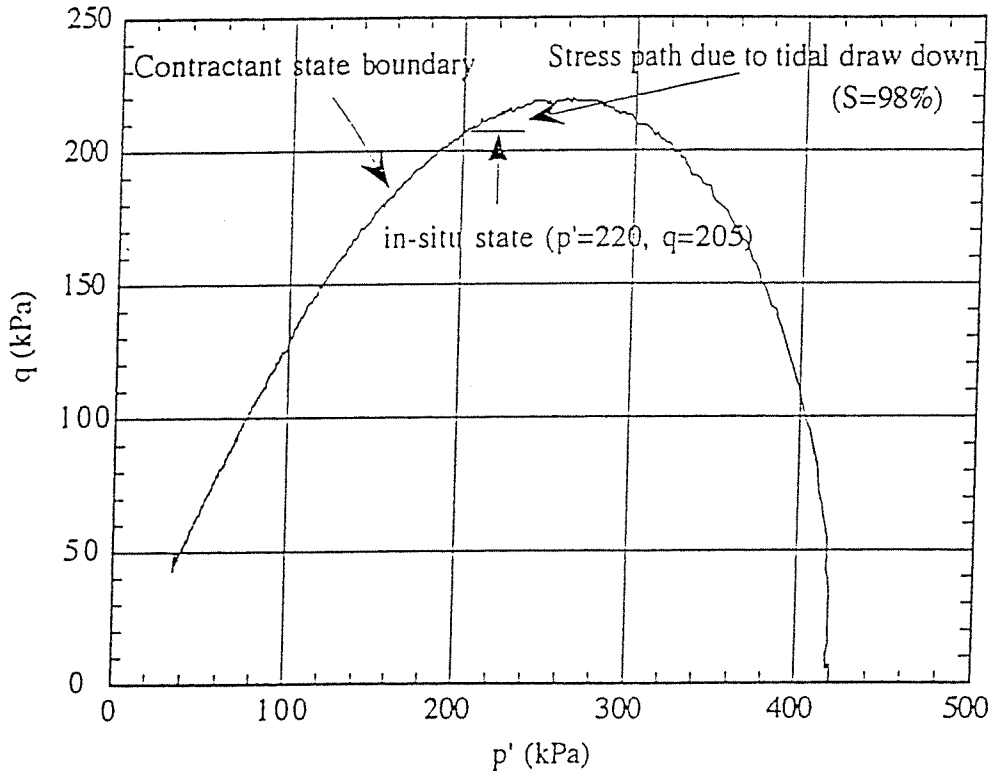

Figure 13. Influence of tidal drawdown on contractant state boundary surface